THE JOURNAL OF PHYSICAL CHEMISTRY C

Article

pubs.acs.org/JPCC

Nanotube Motion on Layered Materials: A Registry Perspective

Inbal Oz,[†,‡] Itai Leven,[†,‡] Yaron Itkin,[†] Asaf Buchwalter,[†] Katherine Akulov,[†] and Oded Hod*[,†,‡]

[†]Department of Physical Chemistry, School of Chemistry, The Raymond and Beverly Sackler Faculty of Exact Sciences, Tel Aviv University, Tel Aviv 6997801, Israel

[‡]The Sackler Center for Computational Molecular and Materials Science, Tel Aviv University, Tel Aviv 6997801, Israel

Supporting Information

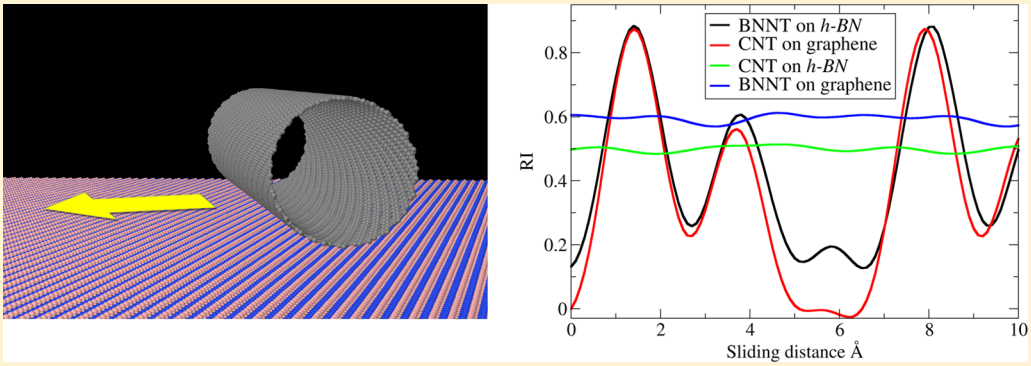

ABSTRACT: At dry and clean material junctions of rigid materials the corrugation of the sliding energy landscape is dominated by variations of Pauli repulsions. These occur when electron clouds centered around atoms in adjacent layers overlap as they slide across each other. In such cases there exists a direct relation between interfacial surface (in)commensurability and superlubricity, a frictionless and wearless tribological state. The Registry Index is a purely geometrical parameter that quantifies the degree of interlayer commensurability, thus providing a simple and intuitive method for the prediction of sliding energy landscapes at rigid material interfaces. In the present study, we extend the applicability of the Registry Index to nonparallel surfaces, using a model system of nanotube motion on flat hexagonal materials. Our method successfully reproduces sliding energy landscapes of carbon nanotubes on graphene calculated using a Lennard-Jones-type and the Kolmogorov−Crespi interlayer potentials. Furthermore, it captures the sliding energy corrugation of a boron nitride nanotube on hexagonal boron nitride calculated using a recently developed interlayer potential for hexagonal boron nitride (*h*-BN). Finally, we use the Registry Index to predict the sliding energy landscapes of the heterogeneous junctions of a carbon nanotubes on *h*-BN and of boron nitride nanotubes on graphene that are shown to exhibit a significantly reduced corrugation. For such rigid interfaces this is expected to be manifested by superlubric motion.

INTRODUCTION

Nanoelectromechanical systems (NEMS) present the ultimate miniaturization of electromechanical devices.[1,2] Their realization has paved the path for the design of molecular scale devices with unique properties and functionality.[3,4] Nanotubes (NTs) have often been suggested to serve as active components in such systems due to their cylindrical geometry and remarkable mechanical and electronic properties.[5−9] Such setups often involve junctions of NTs and atomically flat surfaces where the detailed lattice structure at the interface determines its tribological properties.[10−12] Gaining a clear understanding of the NT−surface interactions has thus been the focus of several recent computational studies exhibiting the importance of a full atomic-scale description.[13] The tool of choice in such studies is often classical mechanics simulations based on dedicated force-fields that are designed to reproduce the properties of specific junctions as obtained either experimentally or via higher accuracy computational methods.[14−17] These provided important insights regarding the interplay between lattice commensurability and preferred NT orientations as well as the different mechanism underlying various types of motion including sliding, rolling, and spinning. While such descriptions are highly valuable for the interpretation of experimental observations and the prediction of new phenomena, they may turn computationally demanding with increased force-field sophistication and system dimensions and tend to blur the atomic-scale origin of tribological phenomena in nanoscale junctions.

Recently, an alternative that quantifies the interlayer registry in rigid interfaces has been proposed for modeling the interlayer sliding energy surfaces of a variety of hexagonal layered materials including graphene,[18] hexagonal boron nitride (*h*-BN),[19,20] molybdenum disulfide,[21] and multilayered nanotubes thereof.[7,22−24] Within this approach, one defines a registry index (RI) as a geometrical parameter that gives a

Received: January 22, 2016
Published: January 22, 2016

DOI: 10.1021/acs.jpcc.6b00651
J. Phys. Chem. C 2016, 120, 4466−4470

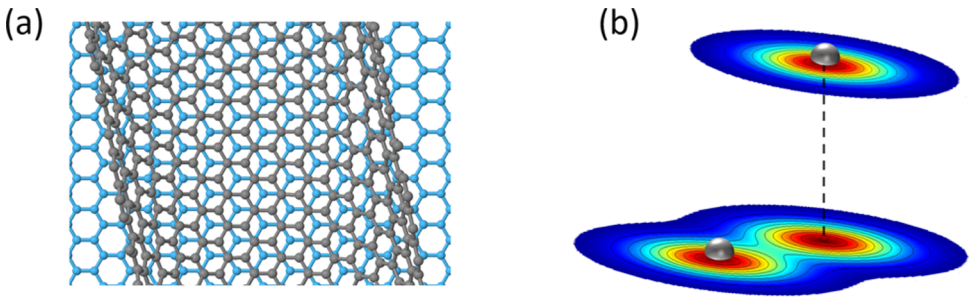

Figure 1. (a) Schematic representation of the optimal configuration of a (20,10) carbon nanotube on a graphene surface. The lower hexagon stripe of the tube is AB-stacked with the underlying flat hexagonal lattice. For clarity, the graphene carbon atoms are colored in cyan, and only the lower half of the tube is presented. (b) Illustration of the projected overlap between two 2D Gaussian functions, one associated with an atom of the tube and another with an atom of the graphene surface.

quantitative measure of the degree of commensurability between two lattices. The method focuses on describing the repulsive Pauli interactions that dictate the potential energy landscape for sliding in these systems via simple circle overlap calculations. Hence, it provides a clear and intuitive description of the origin of sliding energy corrugation with negligible computational cost.

Thus far, the RI was successfully applied to parallel surfaces either flat[18−21,25−27] or curved.[7,22] Here we extend its applicability to treat nonparallel surfaces. As a model system we choose to study the motion of NTs on flat surfaces of hexagonal layered materials. By defining an atom-dependent 2D Gaussian function (replacing the original atomic centered circles) we mimic the effect of reduced Pauli repulsions with increasing distance between atoms belonging to the NT and to the surface. This allows us to fully reproduce the potential energy variations during carbon NT (CNT) spinning, rolling, and sliding on graphene[13] and the sliding motion of a boron nitride nanotube (BNNTs) on *h*-BN as obtained using elaborate force-field calculations. Finally, we use our approach to predict the tribological properties of the heterogeneous interfaces formed between CNTs and *h*-BN or BNNTs and graphene.

COMPUTATIONAL METHODS

In the original RI approach each lattice center was assigned a circle of radius r_i that depended on the atomic identity.[28] In the present implementation, to obtain smoother and more physical registry index surfaces we replace these circles by atomic-centered 2D Gaussian functions whose standard deviations relate to the original circle radii via $\sigma_i = \gamma r_i$, where γ is chosen to reproduce the sliding energy RI landscapes obtained using the original circle-based definition and typically assumes a value of $\gamma = 0.75$ (see Supporting Information). Projected Gaussian overlaps between atomic centers belonging to adjacent surfaces are then analytically calculated to evaluate the local degree of repulsive interactions. A simple formula involving sums and differences of the local overlaps is used to define a numerical parameter aimed to quantify the overall interfacial registry mismatch between the two lattices. To generalize the definition of the RI to nonparallel surfaces one should take into account the intersite distance dependence of the repulsive interactions. To this end, we scale each pair overlap contribution according to the relative distance between the corresponding sites. This follows the spirit of our RI treatment of planar 2*H*−MoS_2 where the circle radii were chosen to reflect the distance between the relevant pair of sublayers.[21]

To demonstrate this, we start by considering the homogeneous junction of a CNT on graphene. First, we assign to each atomic position within the tube and the surface a 2D Gaussian parallel to the graphene surface. The Gaussian standard deviation is chosen to be $\sigma_C = 0.75 \times r_C = 0.75 \times (0.5L_{CC})$, where $L_{CC} = 1.42$ Å is the covalent intercarbon bond in graphene. Next, the projected overlaps between the Gaussians of the tube and those of the surface (see Figure 1b) are calculated according to

$$S_{C_t^i C_g^j} = f(h) \times \int_{-\infty}^{\infty}\int_{-\infty}^{\infty} e^{-(\mathbf{r}-\mathbf{r}_i)^2/2\sigma_i^2} e^{-(\mathbf{r}-\mathbf{r}_j)^2/2\sigma_j^2}\, dx\, dy = f(h) \times \frac{\pi\sigma_i^2\sigma_j^2}{\sqrt{\sigma_i^2+\sigma_j^2}} \times e^{-|\mathbf{r}_i-\mathbf{r}_j|^2/2(\sigma_i^2+\sigma_j^2)} \quad (1)$$

where $\mathbf{r}_i$ and $\mathbf{r}_j$ are 2D vectors representing the projected positions of atoms C_t^i of the tube and C_g^j of the graphene surface on the *XY* plane parallel to the graphene surface, respectively, and $f(h) = H(R - h) \times \exp[-\alpha_g(h - h_g)]$ is a dimensionless scaling factor serving to effectively reduce the interatomic overlap contribution with increasing vertical distance, *h*. With this definition $f(h)$ obtains the value of 1 when the vertical distance equals the equilibrium graphene interlayer distance of $h_g = 3.33$ Å and decays exponentially with a (system-dependent) factor of $\alpha_g = 3.0$ Å^{-1} set to reproduce reference data.[29] The Heaviside step function, $H(R-h)$, serves to cut off all overlap contributions of atoms of the upper tube section, which are assumed to be screened from the surface by the lower tube section. The RI is defined to be proportional to the total overlap area obtained by summing all atomic pair overlaps, $S_{CC}^{tot} = \sum_{i=1}^{N_t}\sum_{j=1}^{N_g} S_{C_t^i C_g^j}$ and normalizes to the range [0,1] similar to its planar system definition[18]

$$RI_{graphitic} = \frac{S_{CC}^{tot} - S_{CC}^{AB}}{S_{CC}^{AA} - S_{CC}^{AB}} \quad (2)$$

To calculate the overlap value at the optimal (S_{CC}^{AB}) stacking mode, we position the tube on the graphene surface such that its translational vector forms an angle of $\left(\frac{\pi}{6} - \theta\right)$, θ being the chiral angle of the tube, with the zigzag graphene direction and the lower hexagon stripe of the tube forming an AB (Bernal) stacking configuration with the graphene surface (see Figure 1). For the worst stacking mode overlap (S_{CC}^{AA}), we merely shift the tube from the optimal position by $-L_{CC}$ in the armchair direction.

DOI: 10.1021/acs.jpcc.6b00651
J. Phys. Chem. C 2016, 120, 4466−4470

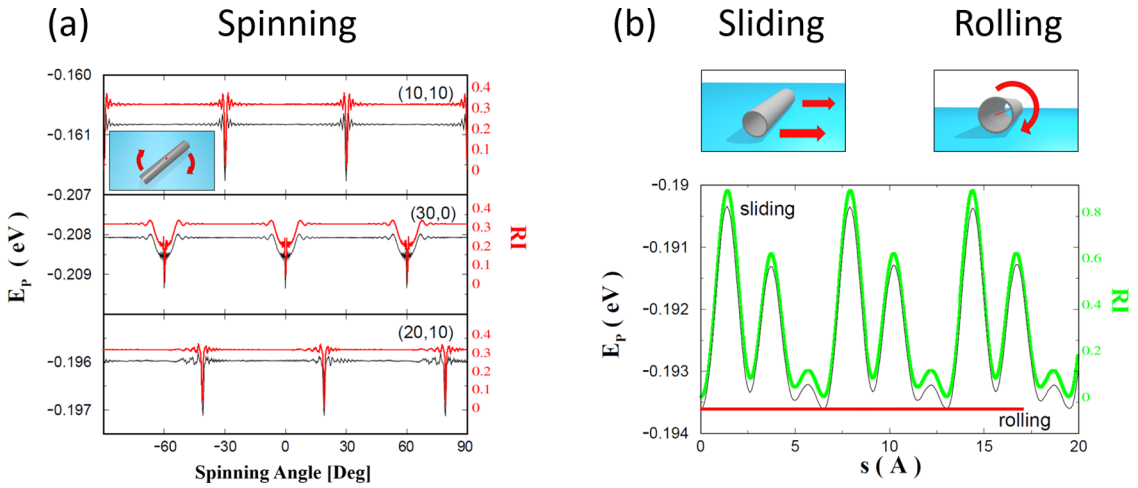

Figure 2. (a) Lennard-Jones energy (black) and RI (red) variations as a function of the spinning angle for (10,10), (30,0), and (20,10) CNTs on graphene (upper, middle, and lower panels, respectively). The RI calculations, performed with NT lengths of 29.5, 38.3, and 22.5 nm for the (10,10), (30,0), and (20,10), respectively, are slightly shifted upward for clarity. Illustration of the spinning motion around the perpendicular axis is presented in the inset of the upper panel. (b) Lennard-Jones energy (black) and RI variations as a function of the sliding (green) and rolling (red) distance for a 56.3 nm long (20,10) CNT on graphene. For clarity, the RI sliding curve is slightly shifted upward. Illustrations of the sliding and rolling motions are provided in the upper left and right insets, respectively. The 2D Gaussian standard deviation for the carbon atoms was taken as $\sigma_C = 0.375L_{CC}$. Sample coordinates for each system are provided in the Supporting Information. The Lennard-Jones reference results were adopted with permission from ref 13. © 1999 American Physical Society.

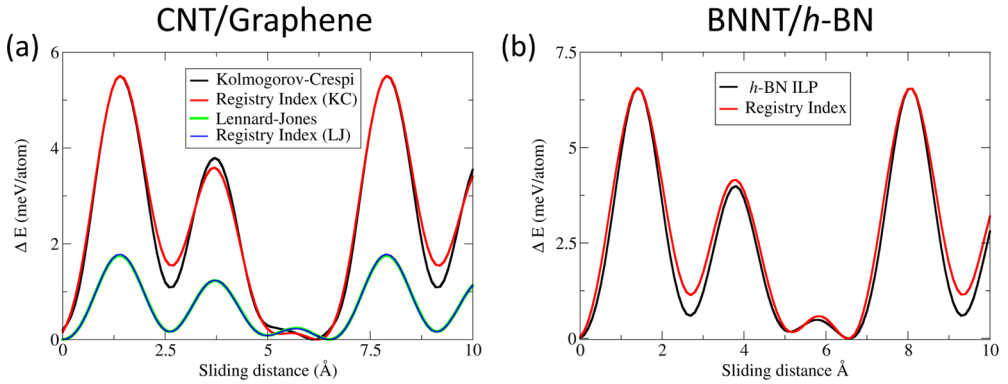

Figure 3. Nanotube sliding energy landscapes calculated using anisotropic interlayer potentials. (a) KC sliding energy (black) and RI (red) variations of a (20,10) CNT of length 56.3 nm as a function of the sliding distance. The LJ landscape (green) and the corresponding RI trace (blue) are presented for comparison purposes. (b) *h*-BN ILP sliding energy (black) and RI (red) landscapes of a (20,10) BNNT of length 56.3 nm as a function of the sliding distances. In the initial configuration the CNT (BNNT) atoms closest to the surface are positioned at the AB (AB_1) stacking mode of graphene (*h*-BN); see Figure 1a. The 2D Gaussian standard deviations used in these calculations are $\sigma_C = 0.375L_{CC}$, $\sigma_B = 0.1125L_{BN}$, and $\sigma_N = 0.375L_{BN}$ for the carbon, boron, and nitrogen atoms, respectively, where $L_{BN} = 1.45$ Å is the covalent boron−nitrogen bond length in *h*-BN. The RI results are multiplied by the appropriate scaling factors and vertically shifted to match the force-field diagrams (see main text).

A similar procedure is used for BNNTs on *h*-BN and for the heterogeneous junctions of CNTs on *h*-BN and BNNTs on graphene with the corresponding RI expressions.[20,30] For these systems as well the Gaussian standard deviations are obtained from the circle radii of the original planar RI definitions with $\gamma = 0.75$, and the corresponding optimal and worst planar stacking modes are used for normalization.[19,25] Specifically, for the heterogeneous junctions normalization procedure, stretched unrolled bilayers with matching lattice constants are used.[25]

RESULTS AND DISCUSSION

We first demonstrate the performance of the suggested approach by showing that it can successfully reproduce the energy landscapes for various types of CNT motion on flat graphene surfaces calculated using classical force-fields. In Figure 2a we compare the energy variations recorded during the spinning of (10,10), (30,0), and (20,10) CNTs on a graphene surface as obtained by Buldum et al. using a Lennard-Jones (LJ) type potential[13] and the corresponding RI changes. As can be seen, for all three systems considered the RI calculation fully reproduces the different force-field results down to fine details with a negligible computational cost. Similarly, when considering the sliding and rolling motions of the (20,10) CNT on graphene (Figure 2b), excellent agreement is achieved between the calculated force-field energy variations and the corresponding RI changes. This excellent agreement between the two types of calculations results from the fact that the dominating interactions determining the calculated energy landscape are of short-range repulsive nature and hence can be readily captured by the simple RI picture, even when the surfaces are not parallel. Importantly, because

DOI: 10.1021/acs.jpcc.6b00651
J. Phys. Chem. C 2016, 120, 4466−4470

we use the same RI parameters and normalization scheme for all motion types, a single scaling factor is sufficient to relate the RI and the force-field results.

To further evaluate the robustness of the RI method for nonparallel surfaces, we repeated the force-field calculations using the anisotropic Kolmogorov–Crespi (KC) potential that was shown to be superior over LJ type expression in describing the interlayer interactions in graphitic systems.[15] Figure 3a presents the corresponding energy variations (black line) during the sliding motion of a (20,10) CNT on a graphene surface. We note that the energy variations are normalized to the number of interacting atoms defined as $N \equiv 2\sum_{i=1}^{N_{tube}} f(h_i)$, where h_i is the vertical height of atom i of the tube above the graphene surface, N_{tube} is the total number of tube atoms, and the factor 2 in front of the sum is introduced to account for the number of interacting surface atoms. The latter is approximated to be identical to the number of tube interacting atoms due to the similar surface atom densities that they exhibit. For comparison purpose, we present the LJ energy variations of Figure 2b normalized using the same procedure. The main differences observed when switching to the KC force-field are (i) increased sliding energy corrugation[31] and (ii) decreased weight of the smaller peak appearing at a sliding distance of 5.7 Å. The former can be accounted for by replacing the RI scaling factor of 1.97 meV/atom appropriate for the LJ sliding corrugation by 6.12 meV/atom for the KC case. The latter results from the anisotropic contribution introduced in the KC potential and requires a slight modification of the RI definition to be captured. To this end, the orientation of the radial p orbital associated with each tube or surface atom is defined as the normal to the surface formed by its nearest-neighboring sites. For each pair of atoms, one residing on the tube and another on the surface, two lateral distances are calculated between the tube atom and the normal to the surface atom and between the surface atom and the normal to the tube atom. The corresponding pair Gaussian overlap is then defined as the average of Gaussian overlaps calculated using the two lateral distances (for more details see the Supporting Information). With this, the RI is able to reproduce both the LJ and KC traces, thus demonstrating its robustness.

Next, we turn to study the motion of a BNNT on a flat *h*-BN surface. To this end, we utilize our recently developed *h*-BN interlayer potential[16] as a benchmark for the RI calculations. Similar to the graphitic case studied above, we consider the sliding motion of a (20,10) BNNT on *h*-BN. In Figure 3b we plot the force-field (black) and RI (red) variations during the sliding motion. The BN system shows general features that resemble those of the graphitic junction with a three-peak periodic structure. We note that the position of the peaks is slightly shifted due to the longer BN covalent bond leading to a larger tube diameter. Here, as well, the RI successfully reproduces the force-field results, with a scaling factor of 8.67 meV/atom. Notably, this good agreement is obtained with an overlap downscale rate identical to the one used for modeling the graphitic systems ($\alpha_{h-BN} = \alpha_g$). This indicates that the dominating interactions are associated with the surface-facing tube atoms, resulting in weak dependence of the results on the choice of overlap downscale rate as discussed above.

Having validated the ability of the RI to describe the energy landscape of nanotube motion on flat hexagonal surfaces of homogeneous systems we may now use it to predict the behavior of the heterogeneous junctions of CNT/*h*-BN and BNNT/graphene. As before, we consider a 56.3 nm long (20,10) nanotube initially positioned, as depicted in Figure 1a. The corresponding RI variations are presented by the green and blue curves in Figure 4 for the CNT/*h*-BN and BNNT/graphene junctions, respectively. For comparison we also present the corresponding results for the homogeneous CNT/graphene (black) and BNNT/*h*-BN (red) systems. Because of the in-plane lattice vectors mismatch between graphene and *h*-BN the heterojunctions exhibit significantly reduced RI variations. We note that care should be taken when comparing the RI landscapes of the various junctions as they require different scaling factors to capture the calculated sliding energy variations. Nevertheless, because the scaling factors of the homogeneous systems differ by <30% and because the corresponding scaling factors of the heterogeneous junctions are expected to be similar or lower (due to the intrinsic lattice vectors mismatch) we can deduce that the latter will present a much less corrugated sliding energy landscape. Therefore, assuming that the interface is clean and that the motion is wearless one may expect lower friction or even superlubric behavior of the rigid heterogeneous junctions.

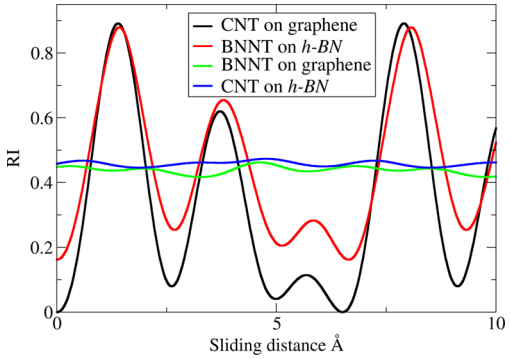

Figure 4. Comparison of sliding RI landscapes for homogeneous and heterogeneous interfaces of 56.3 nm long (20,10) nanotubes and hexagonal surfaces. The tubes are initially positioned at the AB stacking mode with the main axes aligned at an angle of $\pi/6-\theta$ with the zigzag direction (see Supporting Information for sample coordinates). The 2D Gaussian standard deviations of the homogeneous interfaces was taken as $\sigma_C = 0.375L_{CC}$, $\sigma_B = 0.1125L_{BN}$, and $\sigma_N = 0.375L_{BN}$ for the carbon, boron, and nitrogen atoms, respectively. For the heterogeneous junctions the corresponding standard deviations used are $\sigma_C = 0.375L_{CC}$, $\sigma_B = 0.15L_{BN}$, and $\sigma_N = 0.3L_{BN}$.

SUMMARY AND OUTLOOK

In this study, the applicability of the Registry Index method has been extended to the realm of nonparallel rigid interfaces. By rescaling the overlap terms according to the corresponding interatomic distance we were able to capture the energy variations during the sliding, rolling, and spinning motions of CNTs on graphene calculated using both the Lennard-Jones and Kolmogorov–Crespi classical force-fields. Furthermore, the generalized RI was able to reproduce the sliding energy landscape of a BNNT on *h*-BN calculated using the *h*-BN ILP. To model anisotropic interactions introduced by the KC and *h*-BN ILP potentials the calculations of the inter–atomic lateral distance entering the RI overlaps explicitly involve the local surface normal vectors. Furthermore, the circle associated with each atom in the original RI implementation were replaced by Gaussians to allow for smoother and more physical RI landscapes at no extra computational cost. Finally, the sliding

DOI: 10.1021/acs.jpcc.6b00651
J. Phys. Chem. C 2016, 120, 4466–4470

behavior of a CNT on *h*-BN and a BNNT on graphene were studied using the developed approach, indicating that superlubric behavior may be expected to occur at such heterogeneous interfaces.

■ ASSOCIATED CONTENT

Supporting Information

The Supporting Information is available free of charge on the ACS Publications website at DOI: 10.1021/acs.jpcc.6b00651.

Effects of replacement of circle overlaps by 2D Gaussian overlaps and description of the anisotropic pair-overlap calculation. (PDF)

Sample coordinates. (ZIP)

■ AUTHOR INFORMATION

Corresponding Author

*E-mail: odedhod@tau.ac.il.

Notes

The authors declare no competing financial interest.

■ ACKNOWLEDGMENTS

We thank Dr. Yael Roichman for her help with some of the graphics in this paper. This work was supported by the Lise-Meitner Minerva Center for Computational Quantum Chemistry and the Center for Nanoscience and Nanotechnology at Tel-Aviv University. I.O. thanks Ofer Horowitz for helpful discussions.

■ REFERENCES

(1) Ekinci, K. L.; Roukes, M. L. *Rev. Sci. Instrum.* **2005**, *76*, 061101.
(2) Craighead, H. G. *Science* **2000**, *290*, 1532−6.
(3) Shirai, Y.; Osgood, A. J.; Zhao, Y.; Kelly, K. F.; Tour, J. M. *Nano Lett.* **2005**, *5*, 2330−4.
(4) Vives, G.; Tour, J. M. *Acc. Chem. Res.* **2009**, *42*, 473−87.
(5) Cohen-Karni, T.; Segev, L.; Srur-Lavi, O.; Cohen, S. R.; Joselevich, E. *Nat. Nanotechnol.* **2006**, *1*, 36−41.
(6) Nagapriya, K. S.; Goldbart, O.; Kaplan-Ashiri, I.; Seifert, G.; Tenne, R.; Joselevich, E. *Phys. Rev. Lett.* **2008**, *101*, 195501.
(7) Garel, J.; Leven, I.; Zhi, C.; Nagapriya, K. S.; Popovitz-Biro, R.; Golberg, D.; Bando, Y.; Hod, O.; Joselevich, E. *Nano Lett.* **2012**, *12*, 6347−52.
(8) Garel, J.; Zhao, C.; Popovitz-Biro, R.; Golberg, D.; Wang, W.; Joselevich, E. *Nano Lett.* **2014**, *14*, 6132−7.
(9) Levi, R.; Bitton, O.; Leitus, G.; Tenne, R.; Joselevich, E. *Nano Lett.* **2013**, *13*, 3736−41.
(10) Falvo, M.; Steele, J.; Taylor, R. M.; Superfine, R. *Tribol. Lett.* **2000**, *9*, 73−76.
(11) Falvo, M. R.; Taylor, R. M.; Helser, A.; Chi, V.; Brooks, F. P.; Washburn, S.; Superfine, R. *Nature* **1999**, *397*, 236−8.
(12) Chen, Y.; Hu, Y.; Liu, M.; Xu, W.; Zhang, Y.; Xie, L.; Zhang, J. *Nano Lett.* **2013**, *13*, 5666−71.
(13) Buldum, A.; Lu, J. P. *Phys. Rev. Lett.* **1999**, *83*, 5050−5053.
(14) Kolmogorov, A.; Crespi, V. *Phys. Rev. Lett.* **2000**, *85*, 4727−30.
(15) Kolmogorov, A. N.; Crespi, V. H. *Phys. Rev. B: Condens. Matter Mater. Phys.* **2005**, *71*, 235415.
(16) Leven, I.; Azuri, I.; Kronik, L.; Hod, O. *J. Chem. Phys.* **2014**, *140*, 104106.
(17) van Wijk, M. M.; Schuring, A.; Katsnelson, M. I.; Fasolino, A. *Phys. Rev. Lett.* **2014**, *113*, 135504.
(18) Hod, O. *Phys. Rev. B: Condens. Matter Mater. Phys.* **2012**, *86*, 075444.
(19) Hod, O. *J. Chem. Theory Comput.* **2012**, *8*, 1360−1369.
(20) Marom, N.; Bernstein, J.; Garel, J.; Tkatchenko, A.; Joselevich, E.; Kronik, L.; Hod, O. *Phys. Rev. Lett.* **2010**, *105*, 046801.
(21) Blumberg, A.; Keshet, U.; Zaltsman, I.; Hod, O. *J. Phys. Chem. Lett.* **2012**, *3*, 1936−1940.
(22) Hod, O. *Isr. J. Chem.* **2010**, *50*, 506−514.
(23) Hod, O. *ChemPhysChem* **2013**, *14*, 2376−91.
(24) Leven, I.; Guerra, R.; Vanossi, A.; Tosatti, E.; Hod, O. **2016**, submitted.
(25) Leven, I.; Krepel, D.; Shemesh, O.; Hod, O. *J. Phys. Chem. Lett.* **2013**, *4*, 115−20.
(26) Ansari, N.; Nazari, F.; Illas, F. *Phys. Chem. Chem. Phys.* **2015**, *17*, 12908−18.
(27) Zhao, X.; Li, L.; Zhao, M. J. *J. Phys.: Condens. Matter* **2014**, *26*, 095002.
(28) Hod, O. *ChemPhysChem* **2013**, *14*, 2376−2391.
(29) We note that the dependence of the results on the numerical value of this parameter is very weak for the large curvature tubes we consider due to the short-range nature of the relevant interactions.
(30) Leven, I.; Krepel, D.; Shemesh, O.; Hod, O. *J. Phys. Chem. Lett.* **2013**, *4*, 115−120.
(31) Reguzzoni, M.; Fasolino, A.; Molinari, E.; Righi, M. C. *Phys. Rev. B: Condens. Matter Mater. Phys.* **2012**, *86*, 245434.

DOI: 10.1021/acs.jpcc.6b00651
J. Phys. Chem. C 2016, 120, 4466−4470